Improved fabrication of melt electrospun tissue engineering scaffolds using direct writing and advanced electric field control.

Nikola Ristovski[1], **Nathalie Bock**[1,], **Sam Liao**[1], **Sean K. Powell**[1], **Jiongyu Ren**[1], **Giles T.S. Kirby**[1,], **Keith A. Blackwood**[1] **and Maria A. Woodruff**[1]

[1] Biomaterials and Tissue Morphology Group, Institute of Health and Biomedical Innovation, Queensland University of Technology, Brisbane, Australia

ABSTRACT

Direct writing melt electrospinning is an additive manufacturing technique capable of the layer-by-layer fabrication of highly ordered 3d tissue engineering scaffolds from micron-diameter fibres. The utility of these scaffolds, however, is limited by the maximum achievable height of controlled fibre deposition, beyond which the structure becomes increasingly disordered. A source of this disorder is charge build-up on the deposited polymer producing unwanted coulombic forces. In this study we introduce a novel melt electrospinning platform with dual voltage power supplies to reduce undesirable charge effects and improve fibre deposition control. We produced and characterised several 90° cross-hatched fibre scaffolds using a range of needle/collector plate voltages. Fibre thickness was found to be sensitive only to overall potential and invariant to specific tip/collector voltage. We also produced ordered scaffolds up to 200 layers thick (fibre spacing 1 mm, diameter 40 µm) and characterised structure in terms of three distinct zones; ordered, semi-ordered and disordered. Our *in vitro* analysis indicates successful cell attachment and distribution throughout the scaffolds, with little evidence of cell death after seven days. This study demonstrates the importance of electrostatic control for reducing destabilising polymer charge effects and enabling the fabrication of morphologically suitable scaffolds for tissue engineering.

Introduction

The effectiveness of electrospinning as a fabrication technique for tissue engineering is highly dependent on its ability to fabricate scaffolds having both micro and macro-scale structural features optimal for tissue growth. Two main electrospinning methods exist for producing fibres; solution electrospinning and melt electrospinning. Solution electrospinning involves dissolving polymers in a solvent and uses a large electric potential to accelerate solutions from a needle and onto a collector plate. Although this technique is capable of producing fibres with nanometre diameters, solvent evaporation during fibre extrusion induces large instabilities which significantly reduces precise control over fibre placement, commonly known as fibre whipping [1]. Melt electrospinning similarly uses a large electric potential, but produces fibres by liquefying a polymer via heat transfer similar to fused deposition modelling (FDM), a commonly used 3D printing technique. The use of an electric field allows the production of fibres with significantly smaller diameters than can be achieved via a purely mechanical means [2, 3].

Recent work has demonstrated the ability for melt electrospinning to deposit fibres onto a moving collector plate with a great degree of precision in a process called direct writing [4, 5]. By controlling the translation of the collector plate, 2D patterns can be formed which can then be stacked to produce 3D structures with custom internal micro-architectures. However, this technique is limited by the maximum number of layers that can be produced before control over fibre placement is lost due to the accumulation of instabilities [5]. It is hypothesised that a significant source of these instabilities is the build-up of electric charge on the deposited fibres resulting in increasing undesirable net coulombic force acting on the extruding fibre.

In electrospinning, many interacting factors combine to control fibre diameter. These include polymer feed rate [3, 6, 7], applied potential [8], needle tip to collector distance [9, 10], collector translation speed [5], and the mechanochemical properties of the polymer [11]. Due to the viscosity of molten polymer, melt electrospun fibres can be produced with diameters in the micro-scale

range. In addition, the deposition of these fibres is more controllable than solution electrospun fibres which suffer from reduced jet stability due to solvent evaporation [2, 5, 12].

A further advantage of melt over solution electrospinning is that it can produce scaffolds with larger pores sizes which are more suitable for cell infiltration. As solution electrospinning generally produces much smaller fibre networks, in the order of nanometres, the resulting pore sizes after deposition of multiple layers, restrict cell infiltration. This results in large cell populations on the outer layers of the scaffolds, and very limited to no cells in the interior of the scaffold [13]. It has been found that an approximate interconnected pore size of 100-400 μm is ideal for growth of osteoblasts in 3D [14]. This is many orders of magnitude larger than the nano-scale pore sizes of solution electrospun scaffolds, however, direct writing melt electrospinning has the potential to produce scaffolds with customisable pore sizes tailored to the requirements of different cell types.

Combining the principles of additive manufacturing with melt-electrospinning enables the fabrication of 3D structures having configurable fibre diameter, fibre spacing, and laydown pattern. Existing studies on tissue infiltration and growth within 3D melt electrospun fibre networks have demonstrated the importance of pore size and other microstructural characteristics on tissue infiltration and growth [15-18]. Control of fibre placement throughout the entire scaffold is therefore of great importance for the successful application of this technique to tissue engineering.

Although melt electrospinning via direct writing has great promise as a technique for fabricating scaffolds for tissue engineering, it has not yet attracted much attention. The few studies undertaken have identified that precise fibre placement control is affected by the complex interaction of several parameters such as the magnitude of the electric potential between the needle tip and collector, collector speed, and the temperature of the molten polymer [5]. Other important manufacturing properties are the flow rate of the molten polymer and the tip to collector (TTC) distance [12]. As melt electrospinning uses electric potential to draw out fibres from the needle tip, it is hypothesised

that the interaction between the produced electric field and the charge distribution on the surface of the polymer plays a key role in fibre deposition.

The classic melt electrospinning setup involves a positive voltage applied to the tip of the emitter and fibres spun onto a grounded metallic collector plate (Dietmar, 2010?). By distributing the voltage placed on the collector and emitter, it is possible to reduce the amount of charge in the polymer. A negative voltage applied to the collector plate will allow the system to maintain the same potential difference between collector and emitter, but reduce the charge placed on the polymer. It is hypothesised that this change in the electrospinning system will result in greater deposition accuracy for longer periods of time, allowing the production of 3-dimensional constructs.

In this study we produced PCL scaffolds with 90° cross hatched internal microarchitecture to investigate the effect of electrospinning fabrication parameters on scaffold structure order. We also assessed the suitability of the scaffolds for tissue engineering by observing the infiltration and proliferation of murine calvarial osteoblast cells (MC3T3-E1). The scaffolds were fabricated using our custom built direct writing melt electrospinning platform, which uses a negative voltage on the collector plate to reduce residual charge on the fabricated fibres. We found this strategy significantly improved the number of ordered layers achievable over current literature. We also found that fibre spacing affected the maximum number of ordered layers, with greater spacing allowing more ordered layers. The *in vitro* analysis demonstrated a successful infiltration of MC3T3-E1 cells after 7 days in ordered scaffolds with cross hatch microarchitectures. We also observed cell proliferation within the ordered scaffolds did not differ from proliferation in scaffolds with random fibre arrangement.

Materials and Methods

Melt Electrospun Scaffolds

Polymer Preparation

Polycaprolactone (PCL) was obtained from Perstorp (PCL, Capa 6430®, Perstorp UK Limited). PCL pellets were placed in a 2 mL plastic syringe. The syringe was heated in a vacuum oven (- 80 kPa for 30 min at 90 °C) to remove air bubbles.

Melt Electrospinning Device

PCL was electrospun using our novel in-house dual voltage melt electrospinning platform. Figure 1 shows a schematic diagram of the device. A 2 mL syringe loaded with PCL was placed in a heated water jacket at 73 °C. The resulting molten polymer was extruded at a rate of 40 µL/h using a syringe pump (World Precision Instruments, AL-1000). The tip of the extrusion needle and the collector were attached to custom-made isolated power supplies; the tip having a positive voltage, and the collector plate having negative voltage. The collector plate was attached to a motorised translation assembly for controlled x,y,z translation (Velmex, USA). This assembly was attached to a controller (ECG 5-axis board) which was driven via Mach3 software (ArtSoft, USA). The collector plate was translated according to pre-programmed G-code to control the deposition of fibres onto the plate.

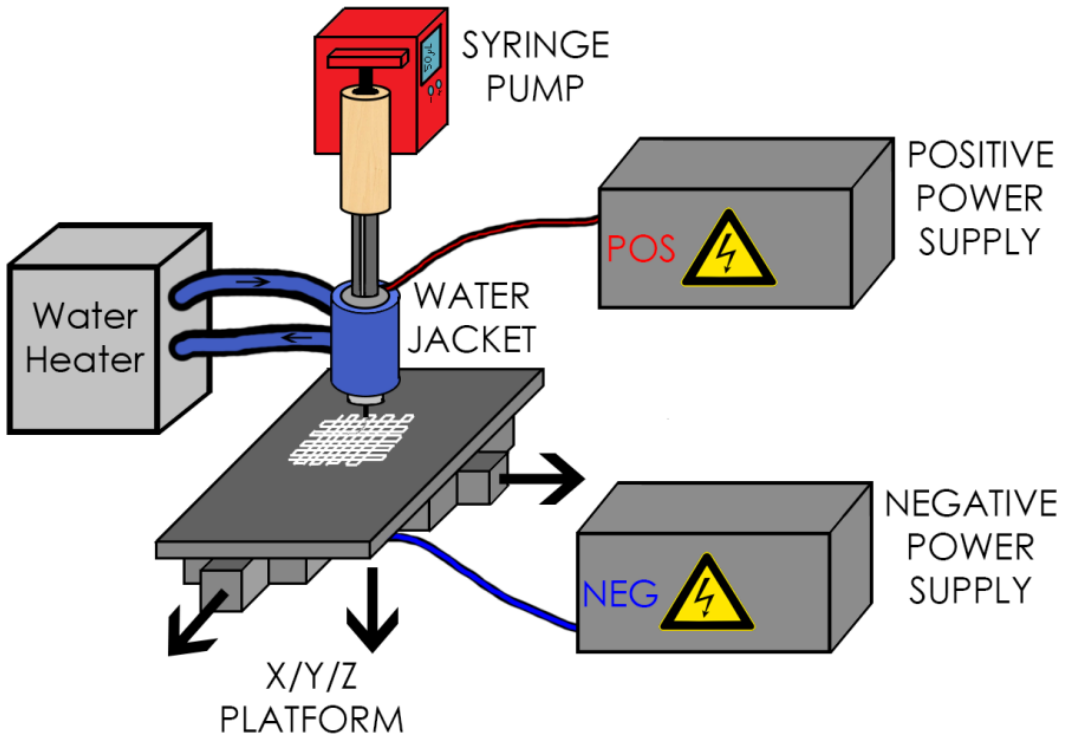

Figure 1: Novel direct writing melt electrospinning platform with dual voltage power supplies for improved fibre deposition control. The negative power supply attached to the collector plate being the defining difference in this system.

Scaffold Production

We separated scaffold fabrication into two phases in order to first determine optimal scaffold production parameters and then assessed the scaffolds for basic cell infiltration and proliferation. The fabrication parameters corresponding to the best performing scaffolds from the first phase were then utilised to produce scaffolds for use in the second phase.

For the ordered scaffolds, we selected a stacked 90° cross-hatched internal microarchitecture with each layer aligned with the x-y plane stacked in the z-axis. As the phase one scaffolds were intended to assess the effect of negative potential on scaffold fabrication control, we held all manufacturing parameters constant for all production and varied only the applied voltages. The following variables were kept constant: temperature (73 °C), extrusion rate (40 µL/h), needle gauge (21 Gauge), stage speed (750 mm/min), needle tip to collector plate distance (10 mm), fibre spacing (500 µm) and electric field strength (1.05 kV/mm). Within this phase we produced 5 groups of 6 scaffolds each using a constant net electrical potential but different positive and negative potentials as shown in table 1.

Table 1: Phase 1 scaffold groups and their corresponding needle tip and collector plate voltages. Six scaffolds were produced for each group.

Group	A	B	C	D	Control
Tip voltage (kV)	Ground	3.5	5	7	10.5
Collector voltage (kV)	-10.5	-7	-5	-3.5	Ground

The scaffolds produced in phase two were intended for assessment of scaffold suitability for cell infiltration and proliferation. We produced two sets of ordered scaffolds having 25 layers and 50 layers, respectively, as well as a set of randomly deposited fibres as shown in table 2. The manufacturing parameters for the ordered scaffolds in this phase were selected as those from group

D in the phase 1 study. The scaffolds for phase 2 were thus manufactured using the same parameters as group D. The random structure scaffold was produced by increasing the needle tip/collector distance to induce fibre whipping. We further fabricated a 90° cross hatched scaffold with 1 mm fibre spacing using the phase 1, group D, manufacturing parameters in order to assess the impact of fibre spacing on scaffold order.

Table 2: Number of scaffolds and structural parameters produced for phase 2 of the study.

		Number of scaffolds fabricated per study		
No. of layers	**Microstructure**	**Live/Dead**	**DAPI/Phalloidin**	**MTT Assay**
25	90° crosshatch	1	1	12
50	90° crosshatch	1	1	12
25	Random	1	1	12

Scaffold Characterisation

SEM Preparation and Imaging

Scanning electron microscopy (SEM) was performed on all scaffolds in phase one, with 6 scaffolds per group, using a Quanta 200 SEM (FEI, USA) to assess microstructure. Prior to imaging, the scaffold was gold sputtered using the Leica EM-SCD005 Sputter Coater for 5 minutes (Leica, Germany). Transverse SEM micrographs of the scaffold (x-y plane) were used to determine the mean fibre diameter and fibre spacing. Sixty fibres were randomly chosen from 5 locations (12 fibres per location) in each scaffold and their diameters were measured. The mean of the diameters was calculated and the standard deviation used for measurement uncertainty. Typical fibre spacing was computed by identifying the relative coordinates of each chosen fibre and using custom Matlab code to compute the average fibre separation. Scaffold layer ordering was also determined from SEM images of scaffold cross-sections (x-z plane).

Distance Transformation Method

Inter-layer fibre alignment is an indicator of the general ordering of the scaffold micro-architecture. A measure for this alignment, or structure order (O_s), can be visualised by considering the length of a line connecting the axial centres of a stacked column of *n* fibres divided by the length of the shortest line connecting the top and bottom fibres in a column and can be calculated via;

$$O_s = \frac{\sum_{i=2}^{n} |\boldsymbol{S}_i - \boldsymbol{S}_{i-1}|}{|\boldsymbol{S}_n - \boldsymbol{S}_1|} \quad (1)$$

where $\boldsymbol{S}_i$ is a vector representing the axial centre of the *i*th fibre in the column. The form of this equation is analogous to the well-known measure of tortuosity, and quantifies stacking order for structures containing n layers, with $O_s = 1$ indicating perfect stacking alignment and $O_s > 1$ for disordered stacking. Centres of fibres where determined using cross-sectional SEM images and data was analysed using MATLAB code.

µCT Imaging and Analysis

Six scaffolds from group C were scanned using a µCT 40 micro computed tomography scanner (Scanco Medical, Brüttisellen, Switzerland) at an energy of 45 kVp, intensity of 177 µA, and 300 ms integration time. Voxel sizes for each scan were 6 µm (isotropic). The scans were analysed using the distance transformation method to determine the average fibre diameter, pore size and pore size distribution throughout the scaffold.

In Vitro *Characterisation*

NaOH Etching

Fibre surface modification was performed to increase the fibre surface roughness and ensure successful scaffold hydration for optimal cell attachment [19]. The hydrophobicity of the PCL was reduced by soaking the scaffolds in 5M NaOH for 1 hour at room temperature. The scaffolds were then soaked in MilliQ water until the supernatant pH dropped to 7.0, and then placed in a desiccator to dry for approximately 24 hours.

Cell Culture

Small sections of scaffolds were extracted using a 6 mm biopsy punch. These were sterilized with 70% ethanol and irradiated with ultraviolet light for 20 minutes each side, all steps were taken consecutively. The scaffolds were divided into three groups; one group of 12 scaffold samples (six per time point) were used for assessing cell proliferation (3-(4,5-dimethylthiazol-2-yl)-2,5-diphenyltetrazolium bromide MTT analysis), a single sample for assessing cell morphology (DAPI/Phalloidin) and a single samples for assessing cell distribution. Murine calvarial osteoblastic cells (MC3T3-E1) were cultured in heat-inactivated α-MEM media (α-MEM, Invitrogen, Australia) with 10% (v/v) foetal bovine serum and 1% (v/v) Penicillin-Streptomycin with a concentration of 10,000 μg/mL. Cell work was performed as previously described by *Ren et al* [20]. An average of 5000 cells were seeded onto each scaffold for proliferation assessment and allowed to attach for one hour in a small volume (50 μl) of media prior to the addition of a further 400 μl of α-MEM media at 37 °C and 5% $C0_2$. An average of ~450,000 cells were seeded with 100 μl of α-MEM onto scaffolds for assessing cell morphology and were allowed to attach for four hours prior to the addition of 400 μl of α-MEM media at 37 °C and 5% $C0_2$. A large quantity was chosen to increase the chances of a homogenous distribution for a qualitative cell morphology assessment and reduce experimentation time. The scaffolds were then incubated at 37 °C and 5% $C0_2$ with the culture media changed approximately every 48 hours, until respective time points were reached.

LIVE/DEAD Staining

Live/dead staining was used, at day 3, as an indicator for positive cell attachment and as an assessment of cell penetration throughout the scaffold. Due to the qualitative nature of this experiment, only one sample was used. The scaffolds were washed twice with PBS. 5 μL stock solutions of Fluorescein diacetate (Invitrogen, USA) (FDA) and propidium iodide (Invitrogen, USA) (PI) where diluted in 5 mL of PBS making a final concentration of 0.67 μg/ml and 5 μg/mL respectively. 2 mL of the FDA and PI solution were added to scaffolds and the cells incubated for 5 minutes in a dark environment at 37 °C. The scaffolds where washed once with 2 mL/well plate of PBS and covered

with fresh PBS. Scaffolds were then transferred onto a glass slide and imaged using the Zeiss Axio M2 (Zeiss, Germany) at excitation levels of λ = 488 nm and λ = 568 nm.

Cell Metabolic Rate Assay

3-(4,5-Dimethylthiazol-2-yl)-2,5-Diphenyltetrazolium Bromide (MTT) assay (Invitrogen, Australia) was used to assess the metabolic activity of cells at days 1 and 7 to check how metabolically active the cells within the scaffolds were. Six samples were taken at each time point. A working solution was produced by diluted 5 mg/mL MTT stock solution with 500 µL of αMEM, for a final working solution of 0.19 µg/mL. The scaffolds were transferred into fresh 48-well plates and 500 µL of fresh media with 20 µL of working solution was added. The cells were then incubated for 4 hours at 37 °C and 5% CO_2. The media was removed and dimethyl sulfoxide (DMSO, Merck, Australia) was added, with 100 µL for day 1 and 200 µL for day 7. The well plates were covered in tinfoil and placed on an orbital shaker for 10 minutes. 100 µL of DMSO was removed from each well and placed in a fresh 96 well plate. Absorption was measured at λ = 540 nm. Absorption data from all empty wells in the well plates was averaged and subtracted from the data. Scaffolds where normalized for the volume of DMSO added to each well plate at the two different time points before comparisons between the two were made.

Cell Morphology and Attachment Staining

A DAPI/Phalloidin assay was used to stain cells at day 3 to qualitatively assess cell adhesion onto the scaffold, with one sample taken. The media was removed and the scaffold was transferred into a fresh 48 well plate. The scaffold was then washed with PBS and fixed in 4% paraformaldehyde for 30 minutes at room temperature. The scaffolds were washed in PBS solution. A 0.2% (v/v) Triton-X-100/PBS solution was added to each well and left for 5 minutes before another wash of PBS. The scaffold was then incubated with 0.5% (w/v) BSA/PBS for 10 minutes and placed in 0.5% (v/v) BSA/PBS with 0.8 U/ml Alexa Fluor Phalloidin and 5 µg/ml DAPI. Following this, the scaffold was

washed in milliQ water once and then stained with Alizarin red S for 5 minutes at room temperature. The scaffold was imaged using a Leica SP5 (Leica, Germany) confocal microscope.

Statistical Analysis

Sample difference was tested using the ANOVA test on SPSS statistics 21 (SPSS. USA), with levene's test used to insure similar variance between groups ($p>0.05$). A Tukey HSD post hoc test was performed on any ANOVA test which had $p > 0.05$ for a pairwise comparison of the subgroups variance.

Results and Discussion

Physical Characterisation

Fibre Diameter and Pore Size

Fibre diameter and pore size are important structural properties of electrospun scaffolds for tissue engineering. Melt electrospinning is capable of producing fibres with diameters from 1 µm to 80 µm [2]. Pore size in the context of tissue engineering scaffolds refers to the average dimension of the spherical fibre free volumes within a scaffold. Although the shapes of the pores vary throughout a scaffold, pore size can be used as an indicator of the typical volumes available for cell infiltration and proliferation. For randomly distributed fibres, the sizes of pores are normally distributed and have a very large standard deviation. By introducing control over fibre deposition, the pore sizes can be controlled and pore size distribution reduced. Controlling pore size is difficult with randomly configured fibres with smaller pores significantly restricting cell infiltration [13].

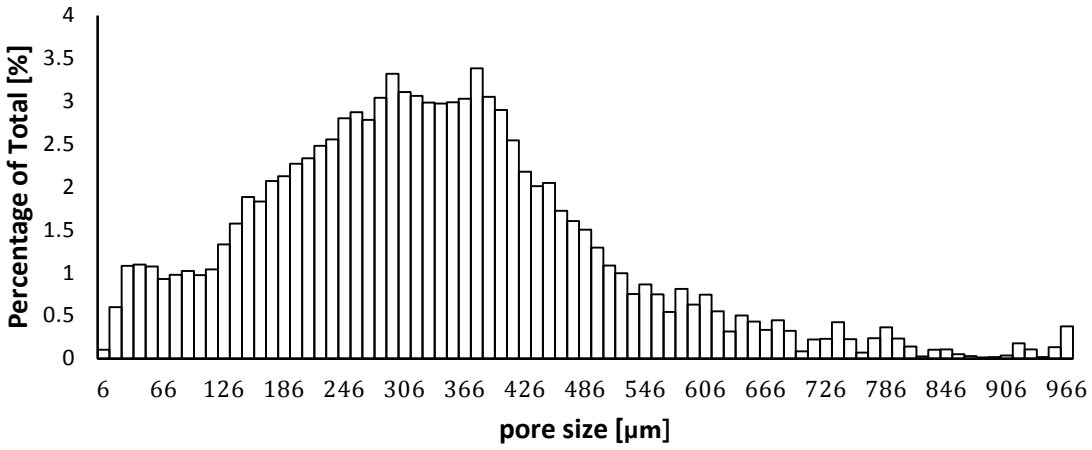

Figure 2: Distribution of pore sizes for group D (+7 kV tip: -3.5 kV collector). The data shows two apparent peaks at 282 µm and 378 µm which can be attributed to the fibre separation in the x-y plane.

Figure 2 shows the pore size distribution of the scaffolds from group D (Needle 7 kV and collector -3.5 kV). This demonstrates the degree of control over fibre ordering with the majority of pores being greater than 100 µm. Ninety degree cross-hatch scaffold architecture results in vertical square-prism shaped pores. Pore size is a measure of the maximum radius of a sphere that can fit into a void space. The maximum spherical pore size in perfectly ordered scaffolds is therefore equivalent to the x-y spacing of the fibres. Consequently, the distribution of pore sizes around this ideal value is due to fibre disorder and is an indicator of fibre deposition control during fabrication.

The standard electrospinning configuration consists of a positive voltage on the needle tip and ground at the collector plate. The value of the chosen tip voltage is known to be a key factor in affecting the diameter of the extruded fibre, with a large potential resulting in the production of thinner fibres. In the present study, we fabricated several scaffolds using different potentials for both the needle tip and collector plate (instead of simply grounding the collector plate) while ensuring that the net potential remained constant. To investigate if the negative potential affects fibre diameter, we measured randomly chosen fibres using SEM images. The results, shown in Fig. 3, indicate that fibre diameter is invariant to the chosen voltage for the needle tip and collector plate and therefore only sensitive to the total voltage between the two.

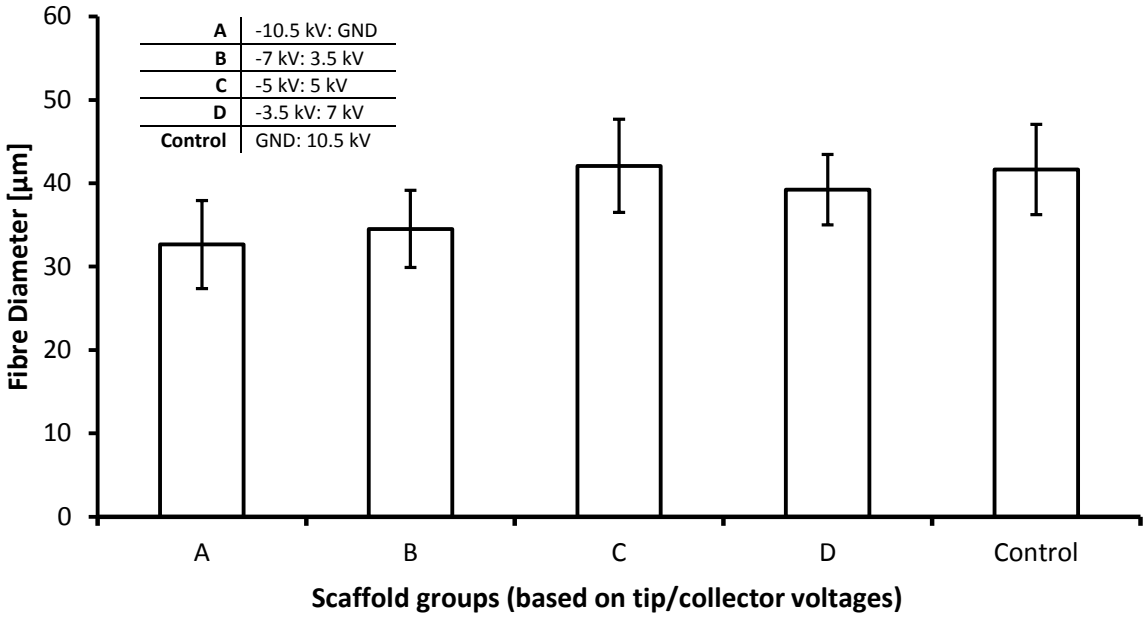

Figure 3: Fibre diameter for different voltage distributions as measured via SEM. Each value was taken by manually measuring the diameter using ImageJ software (n = 48 fibres). The data shows no statistical significance between any groups (p > 0.05).

In addition to average fibre thickness, we also measured fibre diameter variation throughout the scaffolds using µCT images. The average fibre diameter for scaffolds in group D was 20.7 µm ± 3.42 µm. To investigate the suitability of µCT for measuring the diameter of PCL fibres, we compared these results with measurements based on SEM images of the same scaffold. The SEM measurements indicate a mean fibre diameter of 39.2 µm ± 4.3 µm which is approximately twice as large. This discrepancy can be explained by the inability of µCT to resolve actual fibre boundaries due to the low electron density of the polymer.

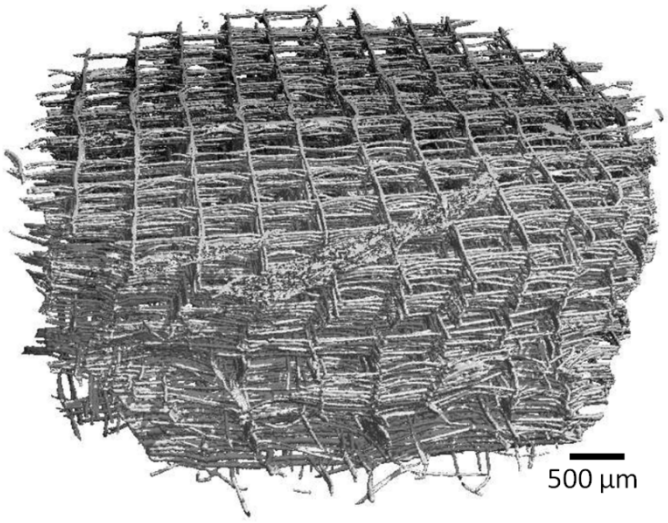

Figure 4: Image of µCT reconstruction of scaffold from group D (+7 kV tip: -3.5 kV collector) with an x-y fibre spacing of 500 µm.

Scaffold Ordering

Controlling the deposition of melt electrospun fibres through direct writing allows the fabrication of tissue relevant scaffolds for use as replacement constructs in regenerative medicine. This control enables the engineering of pore sizes, pore shapes and pore interconnectivity suited to the needs of different cell types. The micron-scale diameters of the electrospun fibres also provides a relatively large surface area to volume ratio compared to thicker fibres, providing good surface for cell attachment. These important factors make direct writing melt electrospinning a promising technique to produce scaffolds for tissue engineering. To assess the degree of control over scaffold fabrication using the direct writing method, we considered two properties; fibre stacking across successive layers, and the maximum number of layers achievable before stacking order was lost.

Fibre Alignment

Inter-layer fibre alignment is an indicator of the general ordering of the scaffold micro-architecture. A measure for this alignment, or structure order (O_s), can be visualised by considering the length of a line connecting the axial centres of a stacked column of *n* fibres divided by the length of the shortest line connecting the top and bottom fibres in a column and can be calculated via;

$$O_s = \frac{\sum_{i=2}^{n} |\boldsymbol{S}_i - \boldsymbol{S}_{i-1}|}{|\boldsymbol{S}_n - \boldsymbol{S}_1|} \quad (1)$$

where $\boldsymbol{S}_i$ is a vector representing the axial centre of the *i*th fibre in the column. The form of this equation is analogous to the well-known measure of tortuosity, and quantifies stacking order for structures containing n layers, with $O_s = 1$ indicating perfect stacking alignment and $O_s > 1$ for disordered stacking. SEM images shown in Fig. 5 are cross sections (x-z plane) of scaffolds from groups A to D and control, and illustrate the effects that different needle tip and collector plate voltages have on stacking order.

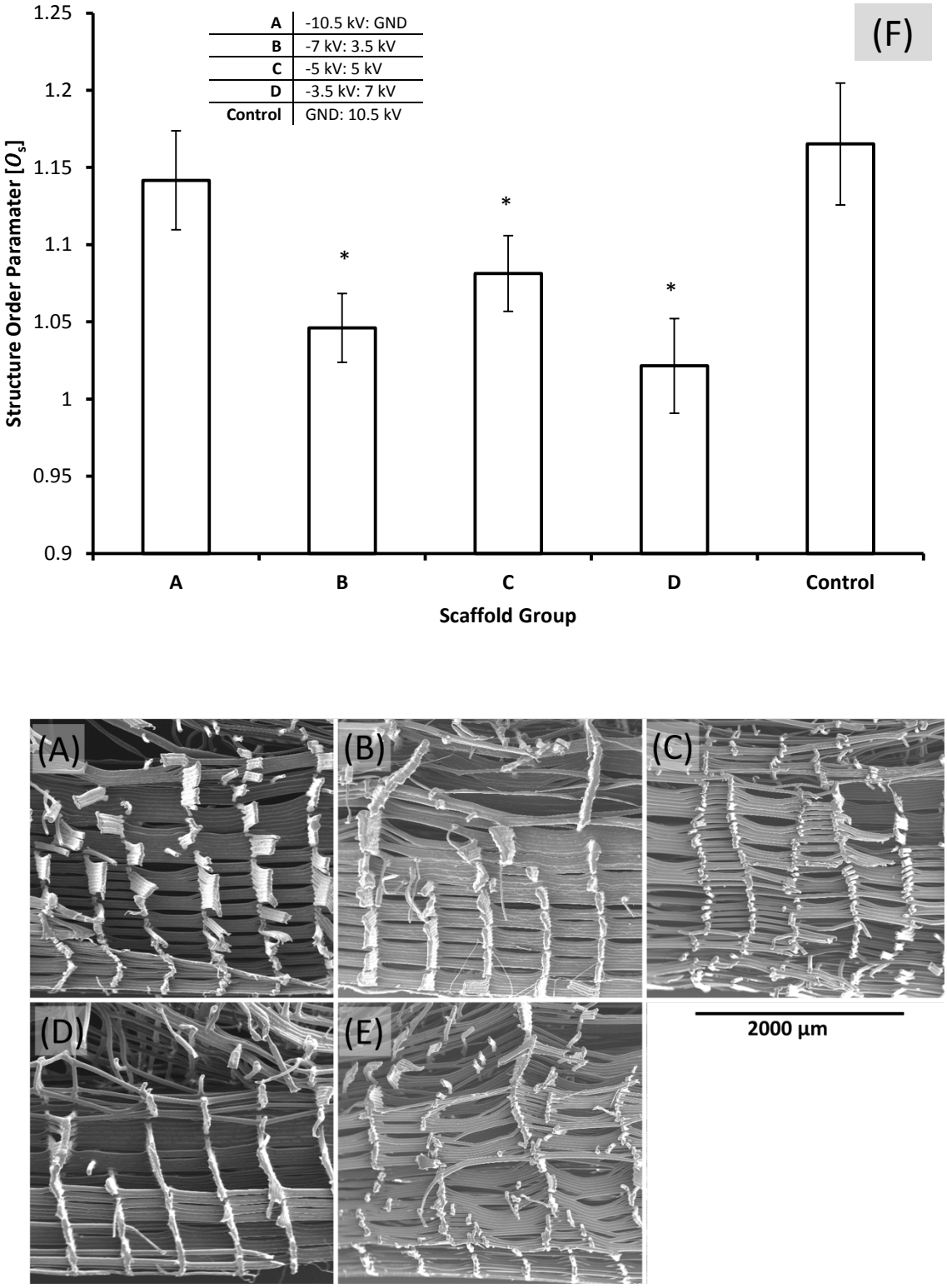

Figure 5: SEM cross-sectional images (x-z plane) of melt electrospun scaffolds with distributions of voltages, varying from 0 to 10.5 kV, between the tip and the collector (see Table 1). (A-D) show scaffolds produced using negative voltage on the collector plate. Scaffold (E) is the control; it is produced by grounding the collector plate. (F) Illustrates the Structure order calculated via Eq. 1 for scaffolds of group

A-D and Control. O_s=1 indicates perfect fibre stacking across all layers, O_s>1 indicates fibre stacking disorder. * indicates a statistical significant mean against control ($p < 0.05$). Uncertainties are computed from the standard deviation.

Using the Eq. 1, we quantified the structure order for scaffolds of groups A-D and the control using 6 different scaffolds from each group; we selected 6 columns from each scaffold in each group and identified the coordinates of the axial fibre centres associated with each column. These coordinates were then used to compute O_S for each column, which was then averaged over the 6 chosen columns to produce a measure of the average structure order for each scaffold. The results shown in Fig. 5 indicate that all scaffolds produced with a negative potential on the collector plate had higher structure order than those produced with the standard grounded collector plate, with scaffolds from groups B and D having the greatest order.

Electrospinning uses the interaction between an electric field and electric charge in the polymer to draw out the fibres. The influence of this interaction is a significant factor affecting the ability to produce ordered structures with micron scale precision. It is hypothesised that during fabrication, the accumulation of charged fibres onto the collector plate results in undesirable net forces acting against the deposition stability. Figure 5 indicates that there is some effect on stacking due to the addition of a negative collector plate. This may be due, in part, to the interaction of charge stored in the polymer and the electric field, resulting in decreased stacking order. This effect is also apparent by observing the decreasing stacking order as a function of stacking height (number of layers) as shown in Fig. 6 for a scaffold comprising 50 layers.

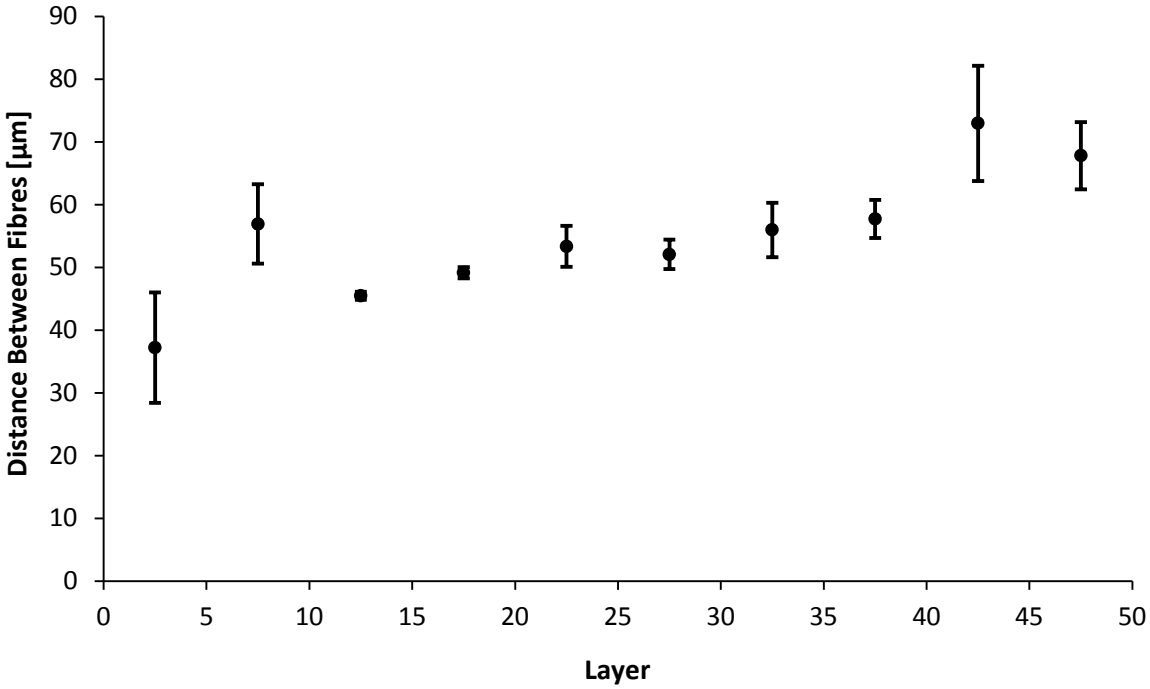

Figure 6: Change in fibre order as the number of layers increases. The vertical inter-fibre distance taken from the axial centre of the fibres indicates fibre order. The results correspond to scaffolds from group D (+7 kV tip: -3.5kV collector).

Another significant parameter affecting stacking order is the intra-layer fibre spacing, which dictates the separation between vertical columns of stacked fibres. The destabilising effect caused by charges in the deposited polymer is proportional to the fibre separation within each layer. To demonstrate this we fabricated two scaffolds similar to group D, but increased the layer fibre spacing from 500 µm to 1 mm (see Fig. 7). SEM images of scaffolds containing 1 mm spacing showed a very clear increase in stacking order which continued through 200 layers. This suggested that intra-layer fibre spacing is also a factor effecting controlled fabrication of melt electrospun scaffolds. In many cases larger spacing is advantageous, for example it is often advantageous to add additional factors to the scaffold to increase bioactivity, for example, the electrospraying of protein loaded PLGA microparticles for growth factor delivery purposes [25, 26].

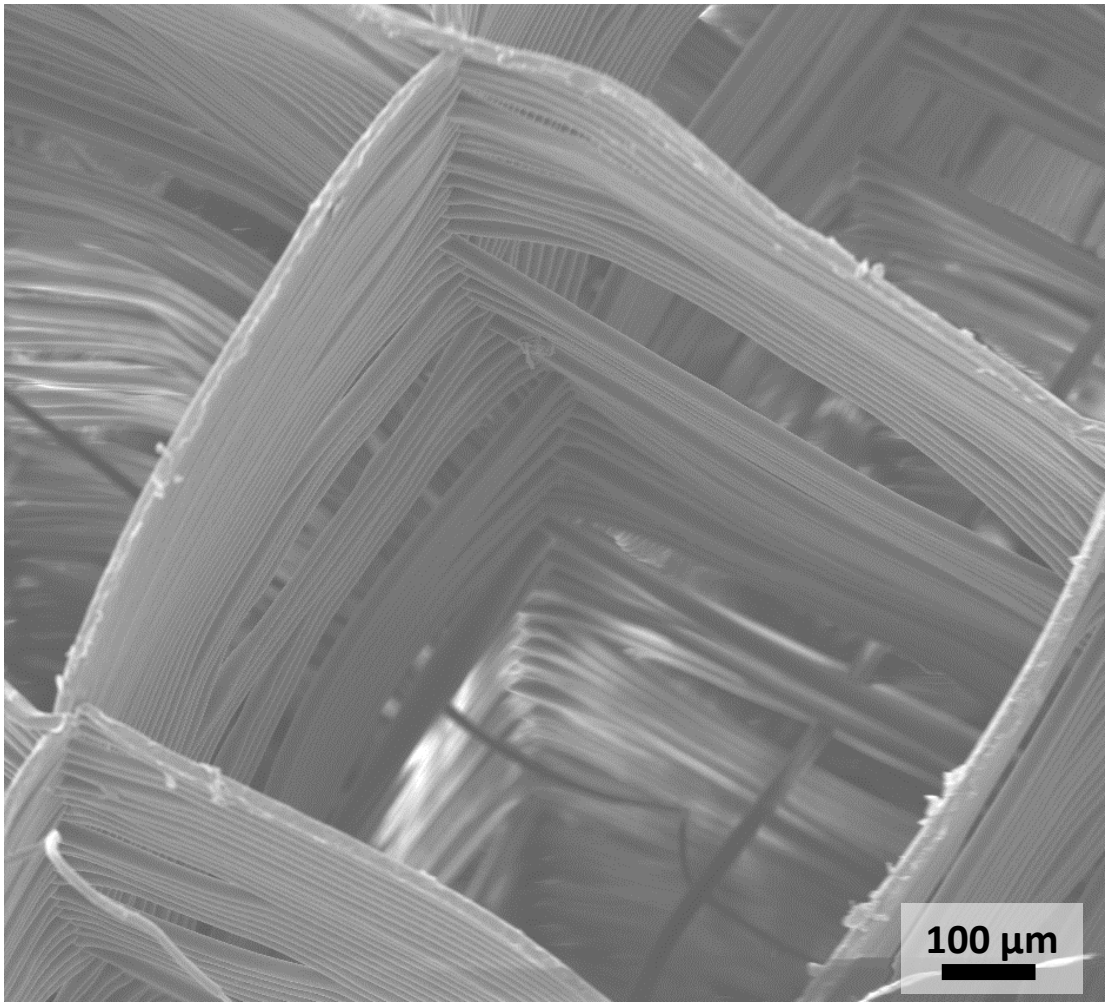

Figure 7: A scaffold with 1 mm fibre spacing produced using group D (+7 kV tip: -3.5 kV collector). The scaffold reached a height of 200 layers (2 mm thickness). This illustrates that by decreasing the density of fibres, the stacking increases.

Zonal Characterisation of structure order

Due to factors discussed previously, there is a limit to the number of layers that can be fabricated in a controlled manner. This limit is influenced by the electric field, charge capacity of the polymer, intra-layer fibre spacing and fibre stacking order. As control of fibre deposition is lost, the structure order transitions through a semi-ordered phase before becoming completely disordered as is apparent in Fig. 8. The ordered region exists in the lower layers of the scaffold (i.e. the first to be deposited) and is distinguished by distinct columns of stacked fibres. Because the columns are clearly identifiable, the stacking order in this region can be quantified using equation 1. The semi-

ordered region describes layers where structure order is still apparent; however distinct columns of fibres are no longer identifiable. In this region, the unwanted forces acting on the extruding fibre caused by the charges on the deposited fibres results in fibres of a given column being completely shifted to an adjacent column. This effect can be seen in the semi-ordered region of Fig. 8 (b) where the second column of fibres from the left of the image ends abruptly. The disordered region is where complete control over fibre deposition is lost and unwanted coulombic forces dominate.

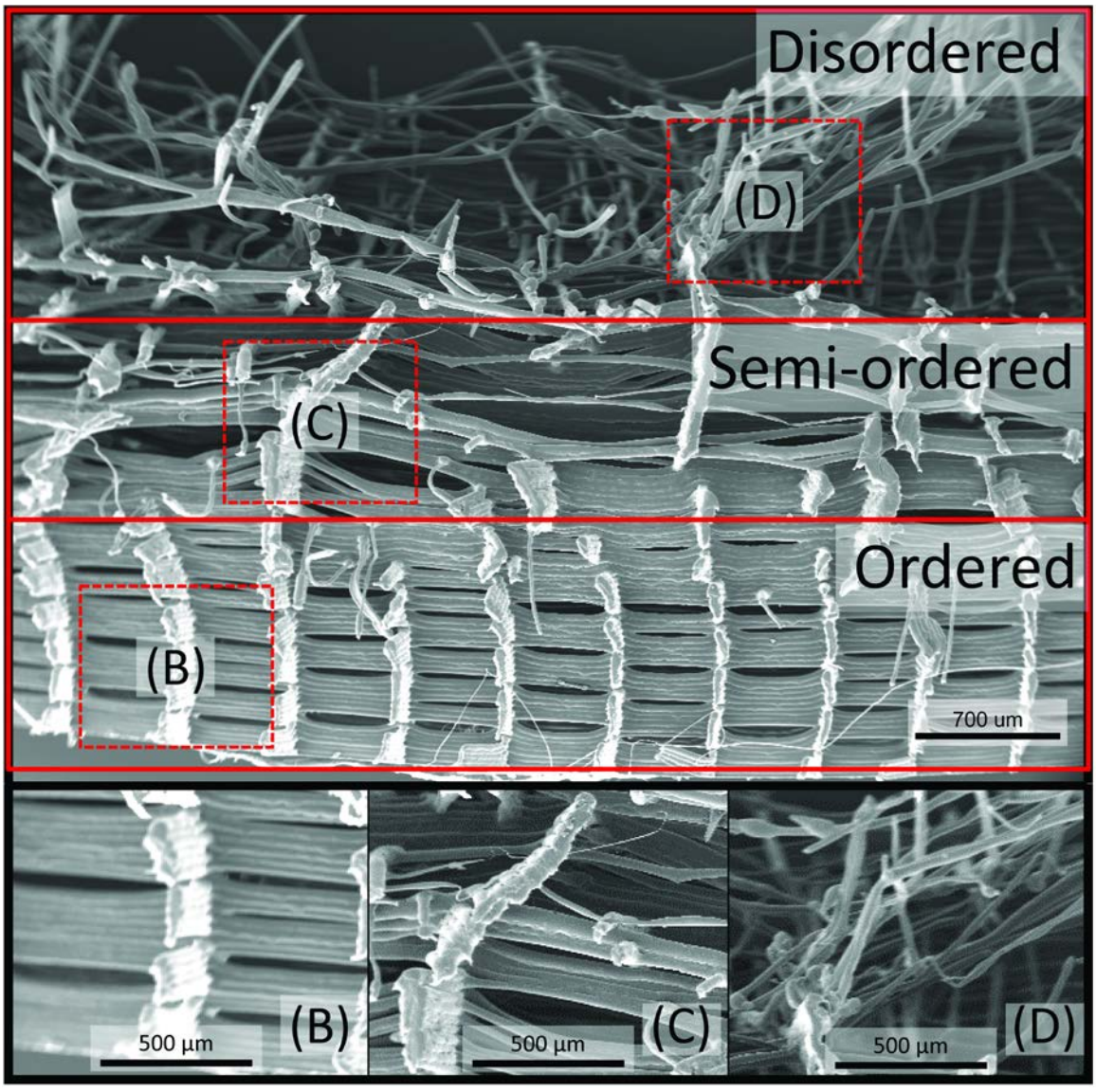

Figure 8: SEM micrographs of a scaffold from group B showing x-z cross section. This illustrates the zonal arrangement of the fibre networks. Sections a, b, and c, are magnified sections of scaffold. The first zone shows a highly ordered structure with large levels of control on fibre deposition. The

secondary zone (semi-ordered) demonstrates some level of control; however the position of fibre deposition is largely influenced by electrostatic forces. The final zone (disordered) shows a complete lack of fibre control with deposition dominated by electrostatic forces.

Fig. 9 shows averaging of the number of layers within the ordered region of scaffolds from groups A-D and the control group. This demonstrates that the use of negative collector potential in melt electrospinning significantly increases the maximum achievable scaffold thickness, with the number of ordered layers in the control group considerably smaller.

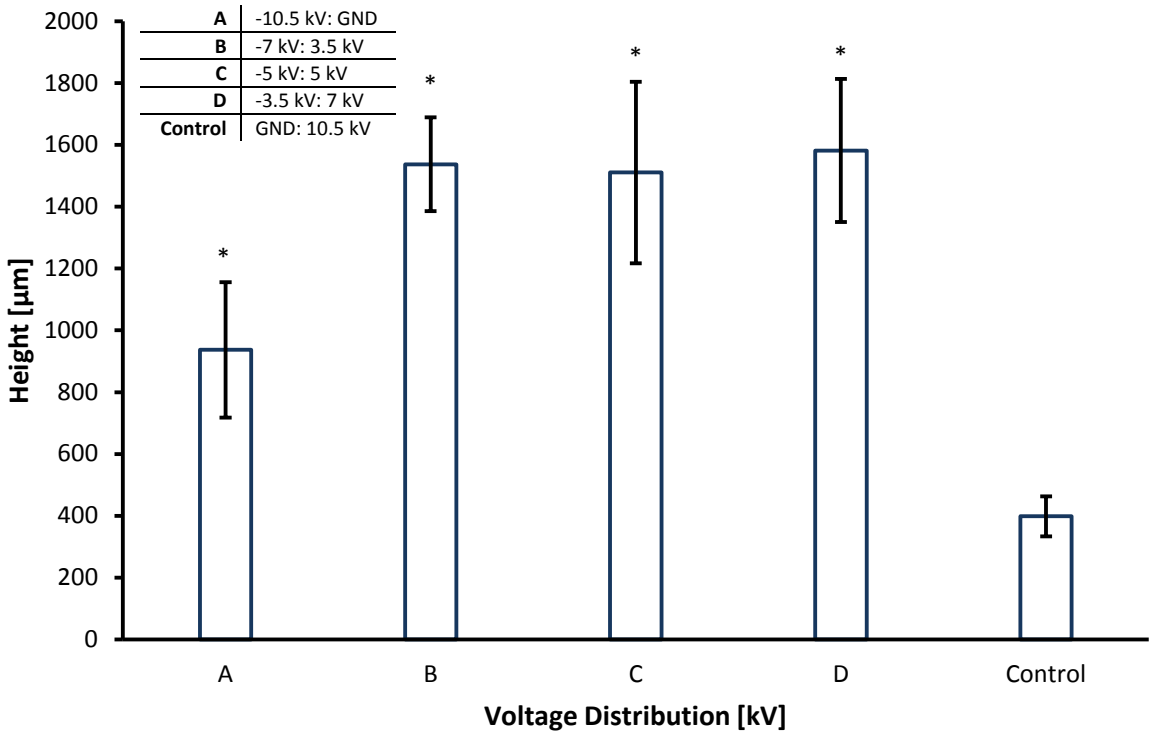

Figure 9: Maximum heights of the ordered zone for scaffolds fabricated for phase 1. Groups A –D had significantly larger ordered zones compared to the control group ($p < 0.05$).

In Vitro Characterisation

To assess the suitability of the electrospun scaffolds for tissue engineering purposes, we performed an *in vitro* analysis of both aligned fibre scaffolds and scaffolds consisting of random fibre networks. The lack of cell infiltration in electrospun scaffolds during cell seeding has been previously

observed, particularly in solution electrospun scaffolds [13, 21]. As direct writing melt electrospinning enables precise control over scaffold microarchitecture, it is possible to tailor the pore sizes to the needs of the cells and significantly improve infiltration and proliferation.

Murine calvarial cells (MC3T3-E1) were seeded on the scaffold with a cell density of 5000 cells per scaffold for 7 days, and 450 000 cells per scaffold for 3 days. To comprehensively evaluate the *in vitro* behaviour of the scaffolds, three studies were completed over the culture period. These studies assessed the viability and distribution of cells within melt electrospun scaffolds with 90° cross-hatched fibre architecture, fibre spacing of ~500 µm, and an ordered thickness of 25 layers and 50 layers. A live/dead stain was used at day 3 to assess the cell viability and as an indicator for cell infiltration in the scaffold. The fluorescent microscopy images in Figs. 10 (A) and (B) indicate that cells are successfully distributed across the surface of the 90° cross-hatched scaffold at day 3.

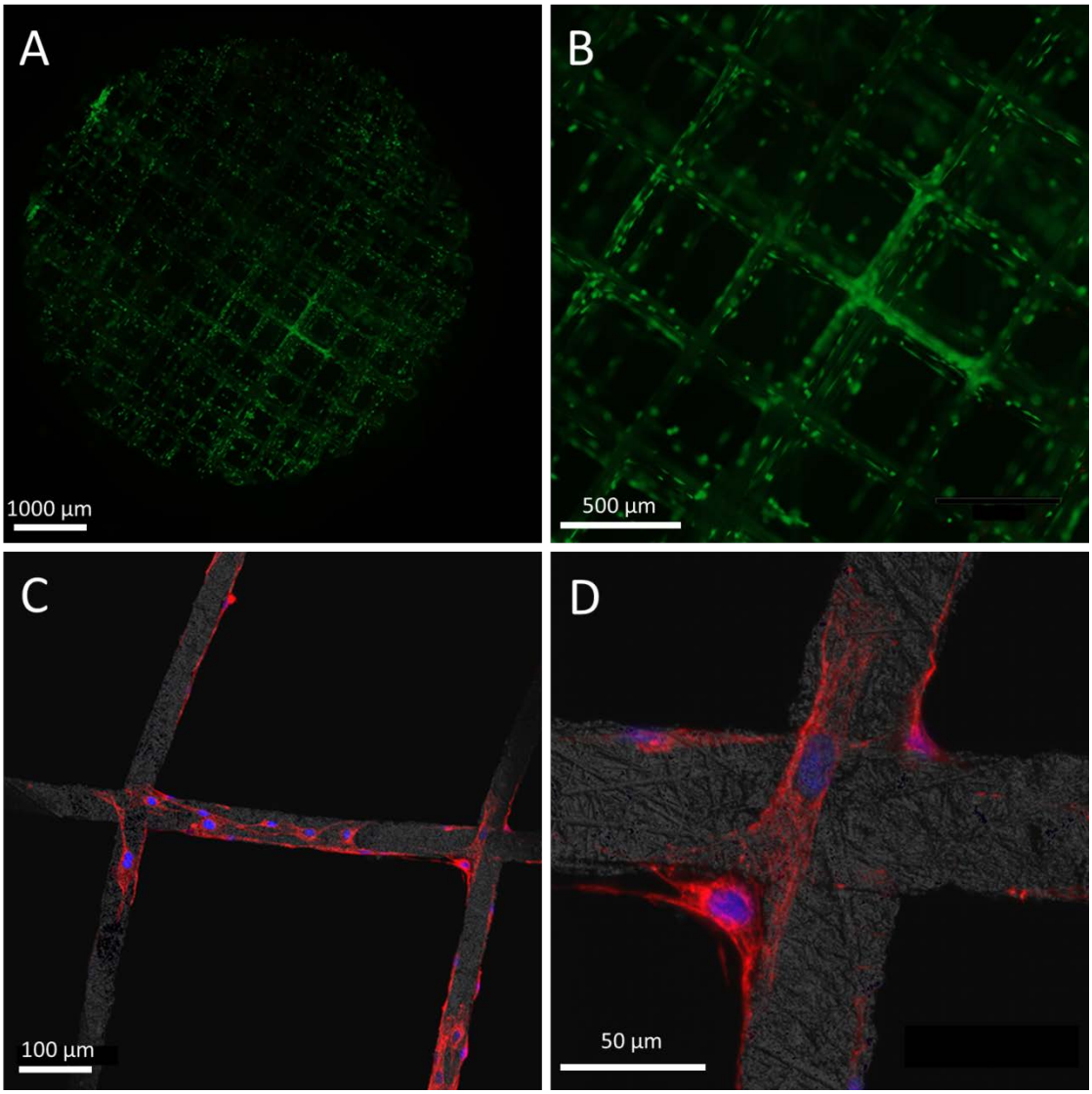

Figure 10: (A) and (B) Cell distribution illustrated using a live/dead stain indicating the presence of cells across the surface of the scaffold. Images (C) and (D) show cell morphology as imaged through a DAPI/Phalloidin stain, illustrating cells attaching and spreading on the scaffold fibres illustrating good cellular interaction.

Studies of cellular morphology were completed to assess the level of cellular interaction within the scaffold. Previous studies have shown mixed results when comparing cellular attachment and morphology between randomly oriented fibre networks and aligned fibre networks [16, 18]. There is some evidence, however, that fibre alignment is influential on cell growth depending on the cell line with fibroblastic, vascular and osteon cells all showing positive responses [16]. In the present study, nuclear/f-actin staining was used to assess cell adhesion and elongation. Figures 10 (C) and (D) show

cells attaching to the scaffold and bridging across the fibres with the active formation of extra-cellular matrix. Comparisons between MTT analysis of cell growth within the 25 layer and 50 layers ordered scaffolds and the randomly structured scaffold showed no difference in cell metabolic activity (n=6) ($p < 0.05$) as seen in Figure 11. This suggests that cell activity was not adversely affected by scaffold ordering.

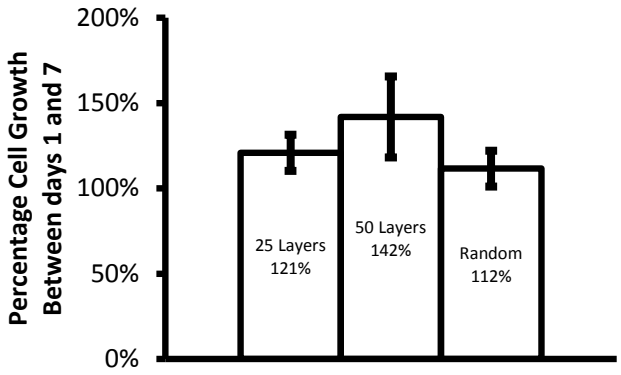

Figure 11: MTT data of the percentage increase in cell growth showing an approximately uniform level of cell proliferation for all scaffolds (n = 6) ($p < 0.05$). Errors bars indicate standard error.

Conclusion

Direct write melt electrospinning offers the ability to fabricate custom 3D tissue engineering scaffolds having highly engineered internal micro-architectures and fibre diameters in the micron-scale. Key to this capability is the use of a large electric potential to draw micron thin fibres from a needle tip and a translatable collector to control their deposition. Control over scaffold fabrication is important for the production of pore sizes that are tailored to the requirements of various cell types. This control also enables the engineering of micro-channels designed to ensure adequate supply of oxygen and nutrients and removal of metabolic waste. Due to electric field instabilities caused by the accumulation of electric charge in deposited fibres, maintenance of this control is difficult beyond a maximum number of layers. This limits the utility of melt electrospun scaffolds for tissue engineering purposes.

We demonstrated that the maximum number of layers can be considerably increased through the novel use of a dual voltage power supply; with a positive voltage on the needle tip and a negative voltage on the collector plate. This offers substantial improvements in scaffold ordering over the standard techniques which use only a single supply and ground. Using the dual voltages, we were able to produce scaffolds with a relatively high degree of ordering and to maintain control over this ordering over significantly more layers than standard grounded collector techniques. We produced highly ordered scaffolds up to 200 layers high (2mm thick) while maintaining precise control over fibre diameter. The resulting scaffolds were seeded with murine calvarial cells to assess their biocompatibility and suitability for tissue engineering purposes and cells attached well and spread throughout the scaffold with little evidence of cell death. The results indicate that the accumulation of charged polymer in fabricated electrospun scaffolds produces an increasing amount of undesirable net forces on the fibre being deposited, thereby reducing deposition control. The use of a negative potential on the collector plate significantly mitigates this effect. Further studies characterising the charges on electrospun polymer fibres during the fabrication process are already underway.

Acknowledgements

This research was supported under the Australian Research Council Linkage Projects funding scheme (LP130100461 and LP110200082). The authors also wish to acknowledge the help of Dr Roland Steck and Ms Patrina Poh for their assistance with μCT analysis, Ms Rachel Hancock and Dr Leonore de Boer for their assistance with SEM imaging and Mr Alex Roeder for his invaluable help with cell culture and staining.

References

[1] C. S. Kong, W. S. Yoo, N. G. Jo, and H. S. Kim, "Electrospinning Mechanism for Producing Nanoscale Polymer Fibers," *Journal of Macromolecular Science, Part B,* vol. 49, pp. 122-131, 2010/01/01 2010.
[2] D. W. Hutmacher and P. D. Dalton, "Melt electrospinning," *Chem Asian J,* vol. 6, pp. 44-56, Jan 3 2011.
[3] A. L. Y. Darrel H. Reneker, "Electrospinning Jets and Polymer Nanofibers," *Polymer,* vol. 49, pp. 2387-2425, 2008.
[4] N. Detta, T. D. Brown, F. K. Edin, K. Albrecht, F. Chiellini, E. Chiellini*, et al.*, "Melt electrospinning of polycaprolactone and its blends with poly(ethylene glycol)," *Polymer International,* vol. 59, pp. 1558-1562, 2010.
[5] T. D. Brown, P. D. Dalton, and D. W. Hutmacher, "Direct writing by way of melt electrospinning," *Adv Mater,* vol. 23, pp. 5651-7, Dec 15 2011.
[6] G. L. B. Koyal Garg, "Electrospinning jets and nanofibrous structures," *Biomicrofluidics,* vol. 5, pp. 1-19, 2011.
[7] C. Vaquette and J. Cooper-White, "Increasing electrospun scaffold pore size with tailored collectors for improved cell penetration," *Acta Biomaterialia,* pp. 2544-2557, 2011.
[8] M. R. Delaram Fallahi, Naser Mohammadi, Behrooz Vahidi, "Effect of applied voltage on het electric current and flow rate in electrospinning of polyacrylontrile solution," *Polymer International,* vol. 57, pp. 1363-1368, 2008.
[9] W. E. Teo and S. Ramakrishna, "A Review on Electrospinning Design and Nanofibre Assemblies," *Nanotechnology,* vol. 17, pp. 89-106, 2006.
[10] D. Sun, C. Chang, S. Li, and L. Lin, "Near-Field Electrospinning," *Nano Letters,* vol. 6, pp. 839-842, 2006/04/01 2006.
[11] D. W. Hutmacher and P. Dalton, "Electrospinning," *Chemistry,* vol. 6, pp. 44-56, 2011.
[12] P. D. Dalton, N. T. Joergensen, J. Groll, and M. Moeller, "Patterned melt electrospun substrates for tissue engineering," *Biomed Mater,* vol. 3, p. 034109, Sep 2008.
[13] B. L. Farrugia, T. D. Brown, Z. Upton, D. W. Hutmacher, P. D. Dalton, and T. R. Dargaville, "Dermal fibroblast infiltration of poly(epsilon-caprolactone) scaffolds fabricated by melt electrospinning in a direct writing mode," *Biofabrication,* vol. 5, p. 025001, Jun 2013.
[14] G. K. Yong Bok Kim, "Rapid-prototyped collagen scaffolds reinforced with PCL/b-TCP nanofibres to obtain high cell seeding efficiency and enhanced mechanical properties for bone tissue regeneration," *Journal of Materials Chemistry,* vol. 22, pp. 16880-16889, 2012.
[15] T. J. Sill and H. A. von Recum, "Electrospinning: Applications in drug delivery and tissue engineering," *Biomaterials,* vol. 29, pp. 1989-2006, 5// 2008.
[16] L. F. Brooke, D. B. Toby, U. Zee, W. H. Dietmar, D. D. Paul, and R. D. Tim, "Dermal fibroblast infiltration of poly(ε-caprolactone) scaffolds fabricated by melt electrospinning in a direct writing mode," *Biofabrication,* vol. 5, p. 025001, 2013.
[17] A. S. Badami, M. R. Kreke, M. S. Thompson, J. S. Riffle, and A. S. Goldstein, "Effect of fiber diameter on spreading, proliferation, and differentiation of osteoblastic cells on electrospun poly(lactic acid) substrates," *Biomaterials,* vol. 27, pp. 596-606, 2// 2006.
[18] M. Chen, P. K. Patra, S. B. Warner, and S. Bhowmick, "Role of Fiber Diameter in Adhesion and Proliferation of NIH 3T3 Fibroblast on Electrospun Polycaprolactone Scaffolds," *Tissue Engineering,* vol. 13, pp. 579-87, Mar 2007 2007.
[19] A. Cipitria, A. Skelton, T. R. Dargaville, P. D. Dalton, and D. W. Hutmacher, "Design, fabrication and characterization of PCL electrospun scaffolds-a review," *Journal of Materials Chemistry,* vol. 21, pp. 9419-9453, 2011.
[20] J. Ren, K. Blackwood, A. Doustgani, P. P. Poh, R. Steck, M. M. Stevens*, et al.*, "Melt-electrospun polycaprolactone strontium-substituted bioactive glass scaffolds for bone regeneration," *Journal of Biomedical Materials Research Part A,* vol. 102, pp. 3140-3153, 2013.

[21] Q. P. Pham, U. Sharma, and A. G. Mikos, "Electrospun Poly(ε-caprolactone) Microfiber and Multilayer Nanofiber/Microfiber Scaffolds: Characterization of Scaffolds and Measurement of Cellular Infiltration," *Biomacromolecules,* vol. 7, pp. 2796-2805, 2006/10/01 2006.